

The effects of slope and slope position on local and upstream fluid threshold friction velocities

Ning Huang,^{1*} Feng Shi¹ and R. Scott Van Pelt²

¹ Key Laboratory of Mechanics on Disaster and Environment in Western China, The Ministry of Education of China, Department of Mechanics, Lanzhou University, Lanzhou, Gansu 730000, P. R. China

² USDA-ARS-Wind Erosion and Water Conservation Research Unit, 302 W, I-20, Big Spring, TX 79720, USA

*Correspondence to: Ning Huang, Key Laboratory of Mechanics on Western Disaster and Environment, The Ministry of Education of China, Department of Mechanics, Lanzhou University, Lanzhou, Gansu 730000, P. R. China. E-mail: huangn@lzu.edu.cn

Abstract

In deserts, dunes are common aeolian landforms, and parallel ridges are common in cultivated land. A computational fluid dynamics (CFD) model is used to simulate a stable wind blowing over slope beds of varying height and coupled with the slope-compensating fluid threshold friction velocity formula. The model accurately reproduced patterns of flow deceleration at the slope toe and stoss flow acceleration. Based on the CFD-based model, quantitative analyses of slope gradient and particle position on the initiation of particle movement are performed. Results indicate that the slope has a great influence on particle saltation in the windward slope, and the initiation of particle movement is particularly sensitive to particle position with respect to the slope. Copyright © 2008 John Wiley & Sons, Ltd.

Keywords: upstream fluid threshold friction velocity; local fluid threshold friction velocity; particle position; flow acceleration

Received 15 January 2007;
Revised 2 December 2007;
Accepted 2 December 2007

Introduction

Aeolian particle transport has a range of impacts including substantial damage to transportation, communication, foundation facilities and degradation of environmental air quality. Aeolian processes also play a major role in landscape formation through the movement of sand dunes, soil and dust uplift, and soil deposition (Raupach and Lu, 2004). Economic and environmental aeolian impacts have motivated research into particle transport mechanisms in order to prevent or mitigate these hazards (Greeley and Iversen, 1985; Shao, 2000; Zhou *et al.*, 2002; Zheng *et al.*, 2004, 2005, 2006). The prediction of a fluid threshold friction velocity, which is defined as the minimum friction velocity required for the aerodynamic forces to overcome the retarding forces, is considered to be a key variable to the understanding of wind-blown sand transport and soil-erosion (Greeley and Iversen, 1985; Iversen and Rasmussen, 1994; Shao, 2000; Raupach and Lu, 2004). Considerable research has been conducted on fluid threshold friction velocity through theoretical analysis, wind-tunnel experiments and field investigations (Bagnold, 1941; Gillette, 1980; Phillips, 1980, 1984; Greeley and Iversen, 1985; Shao and Lu, 2000).

Several theoretical expressions for fluid threshold friction velocity have been derived for soils with uniform and spherical particles spread loosely over an ideal slope. Slope is an important factor that has to be considered in the study of particle entrainment processes, due to the commonly encountered complexities of desert surfaces, including surface ripples and several forms of dunes. Windward and leeward slopes of the dune may be several metres to hundreds of metres in length with observable effects on wind velocity and initiation of particle movement. Ridges are common in cultivated lands and are often used to control erosion by increasing the shelter angle (Potter *et al.*, 1990). Howard (1977) has theoretically analysed the effects of slope on threshold velocity. Based on the rolling model, Iversen and Rasmussen (1994) attempted to include an interparticle force term in the expression for the effect of slope on static threshold, assuming that the fluid threshold friction velocity is related to the diameter of particles, and is also closely related to the slope. If the influence of interparticle cohesive force and the effects of Reynolds number variation are neglected, the ratio of threshold on a sloping surface to that on a level surface is (Howard, 1977; Allen, 1982; Dyer, 1986; Sarre, 1987; Iversen and Rasmussen, 1994):

$$\frac{u_{*f}^2}{u_{*f0}^2} = \cos \theta + \frac{\sin \theta}{\tan \alpha} \quad (1)$$

where u_{*f} (m s^{-1}) is the local fluid threshold friction velocity (LFTFV) on the slope, u_{*f0} is the fluid threshold friction velocity on the level surface, the angle θ is the slope, the angle α is the static friction angle and its value is usually taken as Iversen and Rasmussen's experimental results (Iversen and Rasmussen, 1994). Formula (1) presents the local fluid threshold friction velocity of wind for the initiation of particle movement on slopes with the angle θ . The so-called local threshold friction velocity in this paper means that a particle at a given position on a specific slope will move when the wind velocity at the position attains the force necessary to overcome the static forces. The local fluid threshold friction velocity is different from the fluid threshold friction velocity of upstream air flow, because the wind velocity decelerates at the dune toe and flow accelerates at the windward slope. (Frank and Kocurek, 1996; Lancaster *et al.*, 1996; Wiggs *et al.*, 1996; McKenna Neuman *et al.*, 2000; Parsons *et al.*, 2004a).

Utilizing ANSYS software, we simulated the distribution of wind speeds for a stable wind blowing over slopes. We used these wind-speed distributions to quantitatively analyse the effects of slope as well as particle position on the initiation of particle movement. The results show that besides slope, the slope position also has a great influence on the initiation of particle movement on the bed surface and the threshold friction velocity of the stable upstream air flow decreases as the slope position approaches the crest for a given slope.

The Effect of Slope Angle on the Threshold Friction Velocity

With Equation (1) we can predict the local fluid threshold friction velocity based on different slope angles. To compare the predicted results with experimental results (Iversen and Rasmussen, 1994), the diameter of sand particles is taken as $d = 0.242$ mm. The function curve $f(\theta)$ between the threshold friction velocity and the slope angle θ is shown in Figure 1. It can be seen from Figure 1 that the predicted results agree well with the experimental observations (Iversen and Rasmussen, 1994) and the threshold friction velocity for particles (of a given diameter) increases with increasing slope angles of θ .

Describing the threshold velocity for a given particle diameter d on slope θ is the first step of the process. To obtain the threshold velocity corresponding to particles at different positions on the slope, we must analyse the distribution of wind speeds for a stable wind blowing over the slope.

Simulation of Airflow over a Slope

The $K - \varepsilon$ turbulence model

A commercial computational fluid dynamics (CFD) code, ANSYS, was used in this study. The turbulent flow was simulated with the Navier–Stokes Equation and the $K - \varepsilon$ turbulence model.

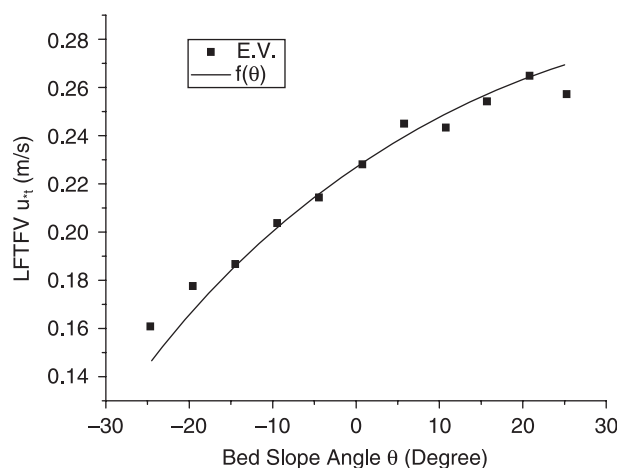


Figure 1. Threshold friction velocity versus bed slope angle.

The conservation equations of mass and momentum of the Reynolds-averaged Navier–Stokes Equation are:

$$\frac{\partial U_i}{\partial x_i} = 0 \quad (2)$$

$$\rho \frac{\partial U_i}{\partial t} + \rho U_j \frac{\partial U_i}{\partial x_j} = -\frac{\partial P}{\partial x_i} + \mu \frac{\partial}{\partial x_j} \left(\frac{\partial U_i}{\partial x_j} + \frac{\partial U_j}{\partial x_i} \right) + \rho \frac{\partial \tau_{ji}}{\partial x_j} \quad (3)$$

where μ is the molecular viscosity, U_i the mean velocity, τ_{ij} the specific Reynolds stress tensor, ρ the air density, and P is the mean static pressure.

The $K - \varepsilon$ model was derived from a theoretical approach simplified to a new form to better serve computational economy, range of applicability and physical realism (Harlow and Nakayama, 1968; Hanjalic and Launder, 1972; Launder *et al.*, 1972; Yakhot and Smith, 1992). The conservation equations for the turbulence kinetic energy K and its dissipation rate ε are:

$$\frac{\partial K}{\partial t} + U_j \frac{\partial K}{\partial x_j} = \tau_{ij} \frac{\partial U_i}{\partial x_j} - \varepsilon + \frac{\partial}{\partial x_j} \left[(v + v_T/\sigma_K) \frac{\partial K}{\partial x_j} \right] \quad (4)$$

$$\frac{\partial \varepsilon}{\partial t} + U_j \frac{\partial \varepsilon}{\partial x_j} = C_{\varepsilon 1} \frac{\varepsilon}{K} \tau_{ij} \frac{\partial U_i}{\partial x_j} - C_{\varepsilon 2} \frac{\varepsilon^2}{K} + \frac{\partial}{\partial x_j} \left[(v + v_T/\sigma_K) \frac{\partial \varepsilon}{\partial x_j} \right] \quad (5)$$

where K is turbulence kinetic energy, ε is the dissipation rate of turbulent kinetic energy, v is the kinetic molecular viscosity, and v_T is the kinetic eddy viscosity and can be computed as:

$$v_T = C_\mu K^2/\varepsilon \quad (6)$$

Based on Boussinesq's assumption, the Reynolds stress tensor can be computed as:

$$\tau_{ij} = v_T \frac{\partial U}{\partial y} \quad (7)$$

The closure coefficients for the $K - \varepsilon$ model are: $C_\mu = 0.09$, $C_{\varepsilon 1} = 1.44$, $C_{\varepsilon 2} = 1.92$, $\sigma_K = 1.0$, $\sigma_\varepsilon = 1.3$. These constants were not optimized in this study and are the original constants proposed by Launder *et al.* (1972).

According to the characteristics of the idealized transverse dune and data of Parsons *et al.* (2004b), this paper establishes triangular physical models from Table I and uses the FLUID141 software module to perform two-dimensional analysis.

Boundary conditions

In order to compare with the results of Parsons *et al.* (2004a) the first model run was conducted to determine an incoming velocity profile that produced a logarithmic distribution profile closely matching that produced by Parsons *et al.* Subsequent model runs were conducted in order to also determine incoming velocity profiles for the logarithmic profile.

The fluid is assumed to be incompressible and pressure is considered to be a relative value. At the outlet profile, the pressure is fixed at zero for all cells and calculated pressures in the domain are defined relative to this. The 'non-slip

Table I. Geometric properties of models 1–4

Model number	Dune height h (m)	Stoss base length L (m)	Stoss angle (degrees)	Lee base length L (m)	Lee slope angle (degrees)
1	0.08	0.56	8.13	0.1280	32.0
2	0.04	0.56	4.09	0.064	32.0
3	0.12	0.56	12.10	0.1920	32.0
4	0.16	0.56	15.95	0.2561	32.0

condition' was applied in the fluid–solid interface. The $K-\varepsilon$ model, which calculates the turbulent kinetic energy k and its rate of dissipation ε based on the assumption that the flow is fully turbulent, is used. The effects of molecular viscosity are negligible and the standard wall function was provided near the boundary.

Model validation

By means of ANSYS software, a commercially available CFD software package, the distribution of wind speed when a stable wind blowing over an idealized transverse dune is simulated using a friction velocity for upstream wind of 0.52 m s^{-1} . To verify our simulations we compare our simulated results with corresponding results of Parsons *et al.* (2004a) and other related results. Figures 2 and 3 show streamwise velocity U (m s^{-1}) and vertical velocity V (m s^{-1}), respectively, around the dune predicted by this paper and that predicted by Parsons *et al.* (2004a). The horizontal axis is along the ground and the vertical axis is the height. The origin of coordinate is the intersection point between the vertical line and the hemline of dune.

From Figures 2 and 3 it can be seen that the results for this paper and those by Parsons *et al.* conform well qualitatively, although different units, grids and calculation domains are used in the two simulations. For example, both simulations by this paper and by Parsons *et al.* (2004a) show that the wind velocity decreases at the toe of dune

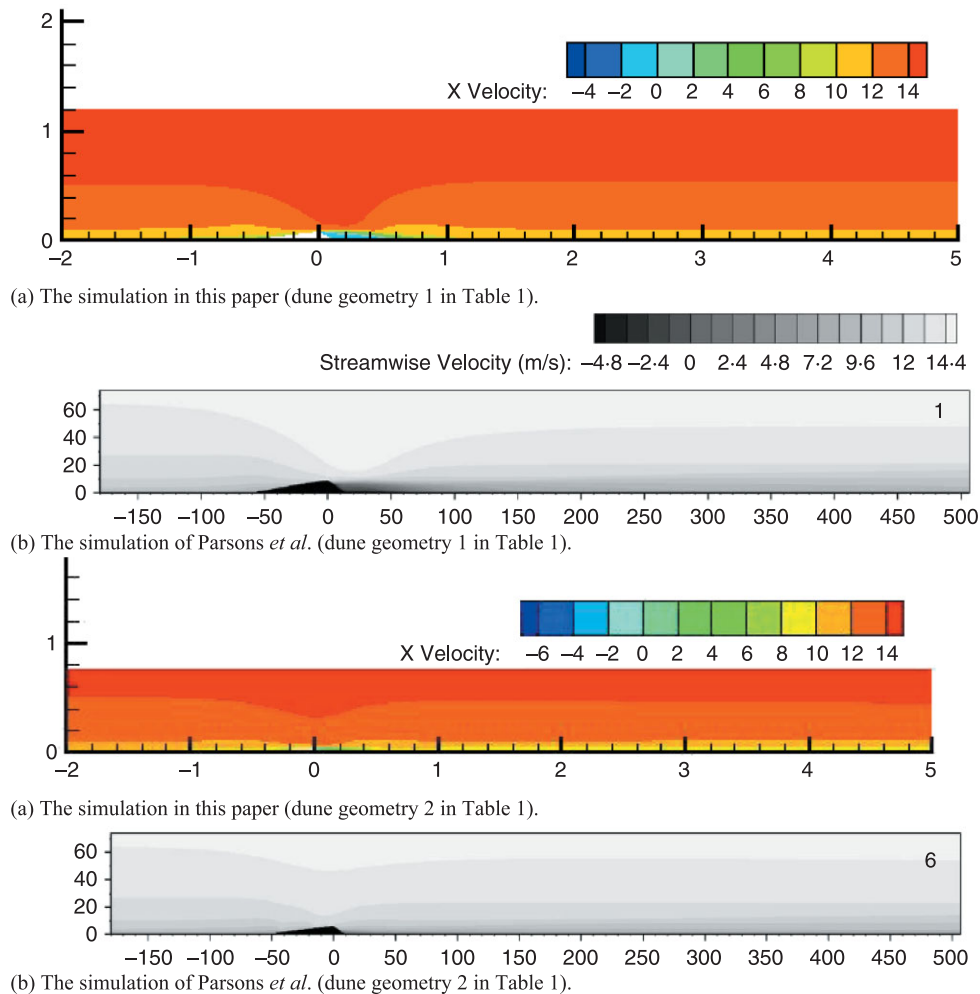


Figure 2. The contour plots of streamwise velocity (U ; m s^{-1}) calculated for two different dune geometry scenarios (dune geometry 1 and 2 in Table I). (a) The simulation in this paper for dune geometry 1. (b) The simulation of Parsons *et al.* (2004a) for dune geometry 1. (c) The simulation in this paper for dune geometry 2. (d) The simulation of Parsons *et al.* (2004a) for dune geometry 2. This figure is available in colour online at www.interscience.wiley.com/journal/esp1

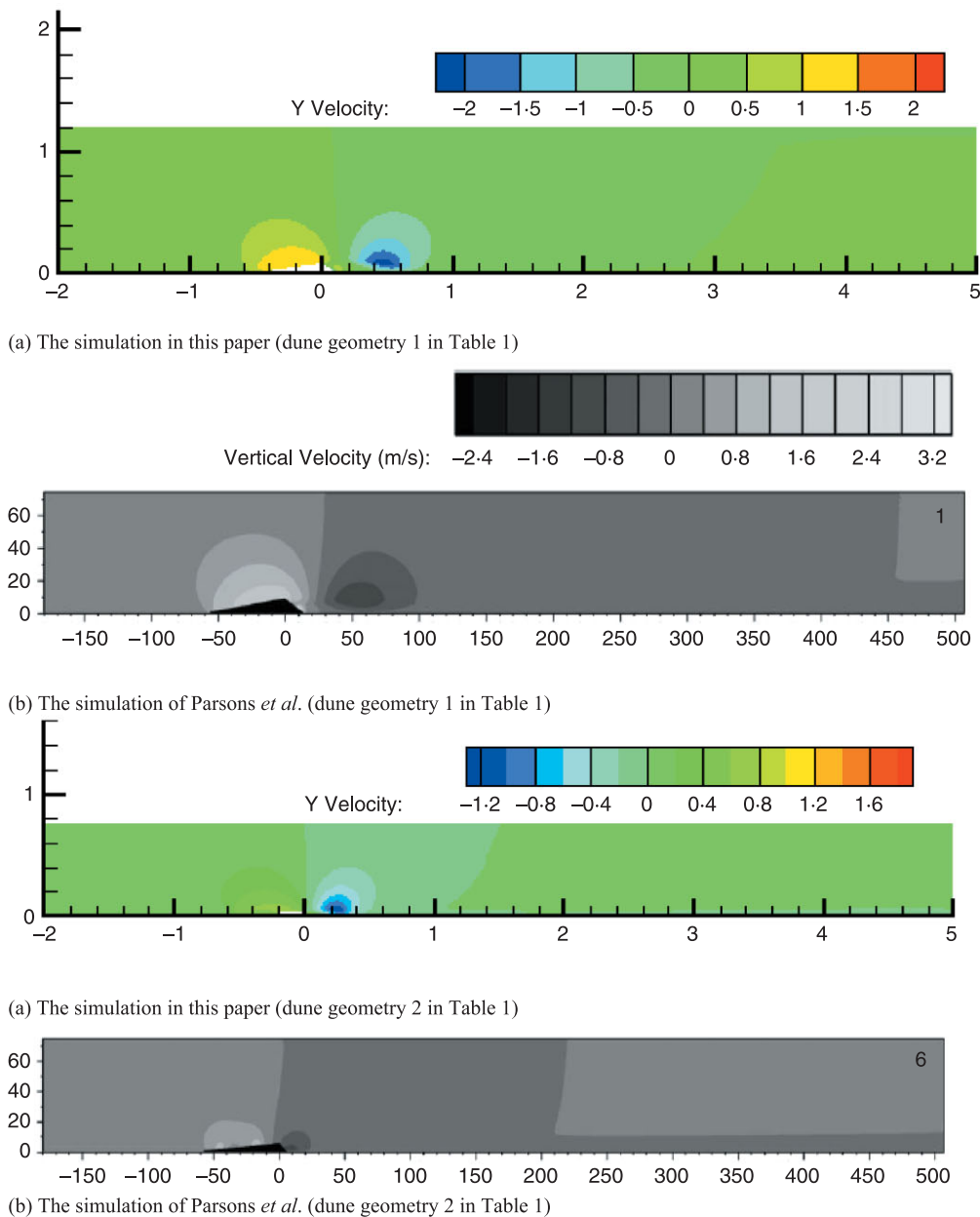


Figure 3. The contour plots of vertical velocity V (m s^{-1}) calculated for two different dune geometry scenarios (dune geometry 1 and 2 in Table I). (a) The simulation in this paper for dune geometry 1. (b) The simulation of Parsons *et al.* (2004a) for dune geometry 1. (c) The simulation in this paper for dune geometry 2. (d) The simulation of Parsons *et al.* (2004a) for dune geometry 2. This figure is available in colour online at www.interscience.wiley.com/journal/espl

because of adverse pressure gradient, increases at the windward slope and reach a maximum value at the crest. These results also correspond to results in other previous investigations (Jackson and Hunt, 1975; Lancaster *et al.*, 1996; McKenna Neuman *et al.*, 1997; Walker and Nickling, 2002; Wiggs *et al.*, 1996). It can be seen from Figures 2 and 3 that it is essential to consider the slope position when establishing the upstream threshold friction velocity formula. The flow reattachment means that the velocity profile along the height resumes a matching logarithmic distribution profile and vertical velocity is close to zero. Figure 3 shows that the point of wind flow recovery for dune geometry 1 is about $26h$ and for dune geometry 2 it is about $31h$. This corresponds well with measurements of $25\text{--}30h$ by

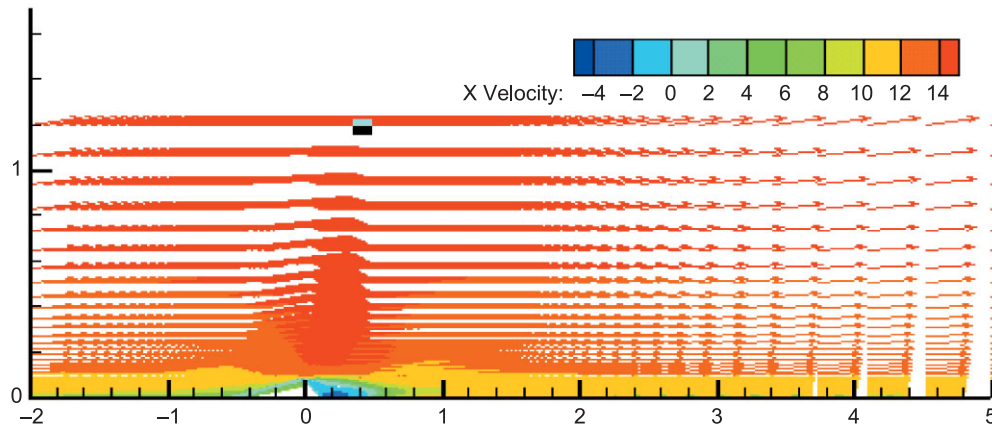


Figure 4. The distribution of wind speed vectors for a stable wind blowing over a dune slope. This figure is available in colour online at www.interscience.wiley.com/journal/esp

Walker and Nickling (2003) and qualitatively conform with the results of Parsons *et al.* (2004a). Therefore, the simulations in this paper are effective.

Figure 4 presents the distribution of wind speed vectors produced by the simulations of this paper. It clearly depicts the separation of flow at the crest. That is, the wind velocity varies greatly on the slope as it accelerates from the toe of the slope and attains a maximum value at the top of slope then decreases on the leeward slope.

Effects of slope and particle position on upstream threshold friction velocity

From Equation (1) it can be seen that the local threshold friction velocity is closely related to slope. Further, the wind velocity varies greatly along the slope when a given upstream wind velocity is blowing over it. Therefore different upstream wind velocities are required to initiate particle movement at different slopes and slope positions. In this section, we first obtain the local threshold friction velocity upwind of an idealized transverse dune with a specific foreslope by Equation (1). Then we calculate the upstream threshold wind friction velocity for a given slope position. We thus determine the upstream wind friction velocity with which the wind velocity at this given position of the slope will attain the local threshold friction velocity by applying the wind velocity simulations discussed previously.

To characterize the position of the particle on the slope (slope position), the value of coordinate x , and the vertical height of the particle above the dune toe expressed by $(x, x \tan \theta)$ are used in Figure 5.

To clearly denote the variation of wind velocity along the slope, we present the numerically derived wind velocity 0.05 m above the bed as a function of slope position when the friction velocity of upstream wind is 0.15 m s^{-1} . It can be seen from Figure 6 that the wind velocity varies greatly and consistently increases from the toe to the crest of the slope. The wind velocity is minimum at the toe of the slope and maximum at the crest of the slope. For example, the wind velocity near the toe of the slope ($x = 0.1 \text{ m}$) is only 4.4 m s^{-1} , but at a higher position of the slope the wind velocity is 5.7 m s^{-1} when $x = 0.5 \text{ m}$. This represents a 29% increase. If the friction velocity of the stable upstream air flow slightly exceeds the local threshold velocity for particles at the top of the slope, the wind velocity at the foot of the slope will most probably be below the threshold velocity. These results agree well with previous research (Frank and Kocurek, 1996; Lancaster *et al.*, 1996; Wiggs *et al.*, 1996; McKenna Neuman *et al.*, 2000; Parsons *et al.*, 2004a,b).

Figure 7 presents the relationship between slope position and upstream threshold friction velocity of the stable upstream air flow, where the particle diameter is 0.1 mm and the dune heights are 0.08, 0.12 and 0.16 m, respectively. For the 0.08 m dune, the upstream threshold friction velocity of the stable upstream air flow needed for the initiation of particle movement at the toe of slope is 0.18 m s^{-1} where $x = 0.05 \text{ m}$. Threshold friction velocity is only 0.15 m s^{-1} where $x = 0.35 \text{ m}$, a decrease of 16% compared with toe of the slope. Similarly, given the same particle diameter and the 0.12 m dune, the upstream threshold friction velocity is 0.20 m s^{-1} at the toe of slope where $x = 0.05 \text{ m}$, but for particles at the crest of slope ($x = 0.35 \text{ m}$), the upstream threshold friction velocity is only 0.15 m s^{-1} , a 23% decrease. Again, given the same particle diameter and the 0.16 m dune, the upstream threshold friction velocity is 0.22 m s^{-1} at the toe of slope where $x = 0.05 \text{ m}$, but for particles at the crest of the slope ($x = 0.35 \text{ m}$), the threshold friction velocity is only 0.16 m s^{-1} , a 28% decrease. When the particle diameter is 0.2 mm, it can also be seen from Figure 7 that the

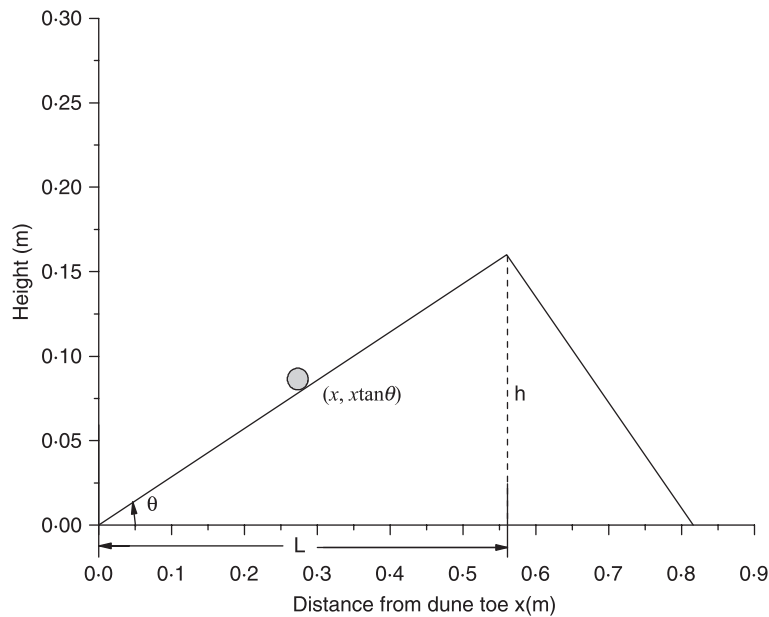


Figure 5. The coordinates to characterize the position of a particle on a fixed slope θ . To characterize the position of the particle on the slope, the value of coordinate x , and the vertical height (h) of the particle above the dune toe expressed by $(x, x \tan \theta)$ are required.

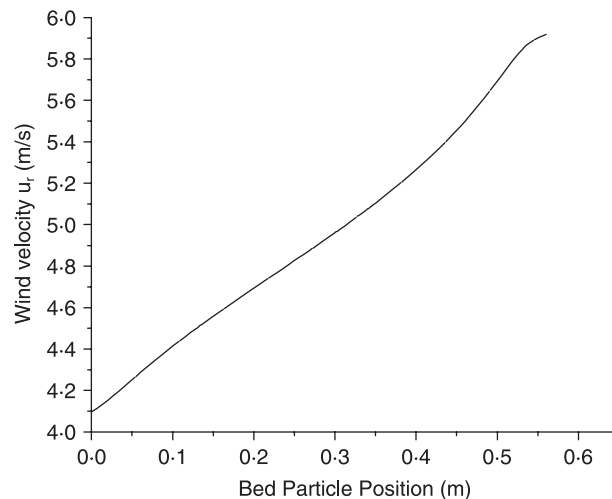


Figure 6. The wind velocity 0.05 m above the bed versus slope position.

upstream threshold friction velocity decreases rapidly along the slope. These results demonstrate that the upstream threshold friction velocity decreases rapidly along the slope, and therefore, particle movement will begin at the crest or near the top of a slope before movement is observed at the toe of the slope. Sand movement is not easy to initiate at the toe of the slope, whereas the particles near or at the crest of a slope are readily set into motion. These results indicate that it is necessary to consider the particle position in calculation of fluid threshold friction velocity on the stoss slope.

From Figure 7 it can be seen that when the value of x is 0.05 m and particle diameter is 0.1 mm, the upstream threshold friction velocities are 0.18, 0.20 and 0.22 m s⁻¹ for the 0.08 m, 0.12 m and 0.16 m dunes, respectively. This represents a reasonably linear increase of threshold friction velocity at a given height above the slope toe with increasing dune height.

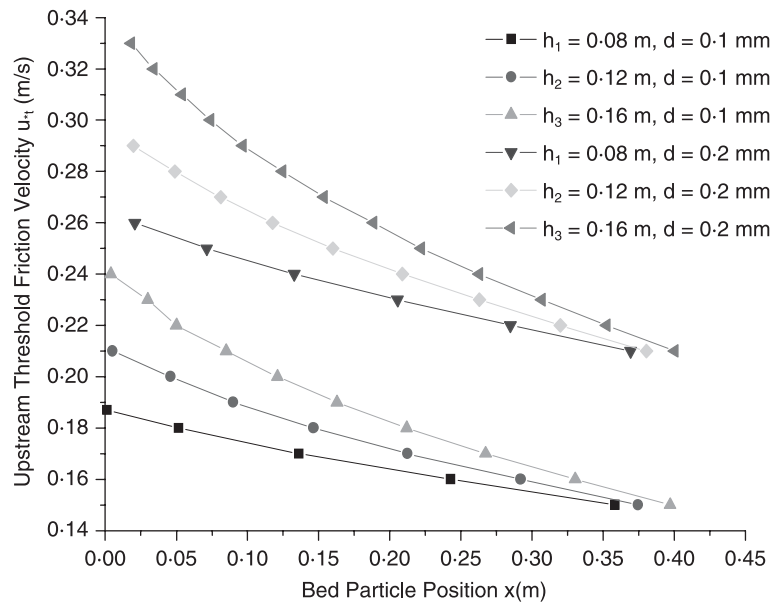


Figure 7. Upstream threshold friction velocity versus slope position for 0.1 mm and 0.2 mm diameter particles.

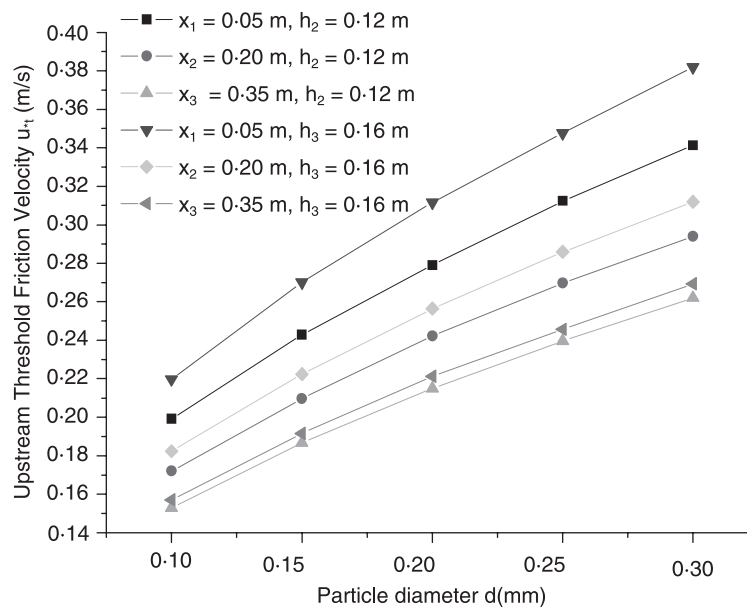


Figure 8. Upstream threshold friction velocity versus particle diameter for 0.12 m and 0.16 m dunes.

The six curves in Figure 8 present the relationship between the upstream threshold friction velocity and the particle diameters for particles at slope positions of $x = 0.05$, 0.20 and 0.35 m for the 0.12 m and 0.16 m dunes, respectively. When the height of the dune is 0.12 m, the upstream threshold friction velocity of the upstream air flow is 0.1992 m s^{-1} for the particles at the toe of the slope ($x = 0.05$ m), with particle diameter of 0.1 mm the upstream threshold friction velocity is 0.3413 m s^{-1} for the 0.30 mm diameter particles at same the value of x , a 71.34% increase. Near the crest of the slope ($x = 0.35$ m), the upstream threshold friction velocity of the upstream air flow is only 0.1529 m s^{-1} for the 0.1 mm particles and 0.262 m s^{-1} for the 0.3 mm diameter particles at same the value of x , a 71.35% increase. These

results indicate that the upstream threshold friction velocity increases rapidly with the particle diameter for particles at the same slope position and strongly resembles findings for a flat surface.

Figure 8 also shows that the upstream threshold friction velocity is 0.1992, 0.172 and 0.1529 m s⁻¹ when $x = 0.05$, 0.20 and 0.35 m, respectively, for particles of 0.1 mm diameter and 0.12 m dunes. For 0.3 mm diameter particles the upstream threshold friction velocity at the toe of slope ($x = 0.05$ m) is 0.3413 m s⁻¹, whereas at the crest of the slope ($x = 0.35$ m), the upstream threshold friction velocity is only 0.262 m s⁻¹, and 0.2939 m s⁻¹ at $x = 0.20$ m. Similarly, when the influence of particle diameters and slope position on the upstream friction velocity necessary to initiate movement on these height dunes can clearly be seen for 0.16 m dune. These data demonstrate well that the upstream threshold friction velocity for particles on a given particle diameter increases with increasing the value of the slope position x .

Conclusions

Using formula (1) to predict the local fluid threshold friction velocity (LFTFV) to initiate particle movement on sloping beds, our calculated results show that the LFTFV of the particle movement increases with increasing slope angle. These results agree favourably with experimental results (Iversen and Rasmussen, 1994) for particles on a slope. We also simulated the distribution of wind speeds resulting when a stable air flow blows over an idealized transverse dune by means of ANSYS software. Based on the numerical results of the distributions of wind speed on the slope, the effects of slope position and particle diameter on the upstream friction velocities necessary to initiate particle movement are quantitatively analysed. The results show that the slope position has a great influence on the initiation of particle movement on the bed surface and the threshold friction velocity of the stable upstream air flow decreases as the slope position approaches the crest. Therefore, the effects of both slope angle and particle position have to be taken into consideration when calculating the upstream friction velocity necessary to initiate particle movement on a slope. The upstream threshold friction velocity increases rapidly with the particle diameter at the same slope position and strongly resembles findings for a flat surface.

Acknowledgements

This research work was supported by a grant of part from the Key Project of NSFC (Grant No. 10532040), the National Natural Science Foundation of China (Grant No. 40571018; 10772073), the New Century Outstanding Talent of the Ministry of Education of China, and the Science Fund of the Ministry of Education of China for PhD Program (Grant No. 20060730014). The authors sincerely appreciate this support. The authors also thank the anonymous reviewers and editors for their thoughtful comments which helped to improve and clarify the manuscript.

References

- Allen JRL. 1982. Simple models for the shape and symmetry of tidal sand waves: (1) statically stable equilibrium forms. *Marine Geology* **48**: 31–49.
- Bagnold RA. 1941. *The Physics of Blown Sand and Desert Dunes*. Methuen: London.
- Dyer K. 1986. *Coastal and Estuarine Sediment Dynamics*. Wiley: New York.
- Frank A, Kocurek G. 1996. Airflow up the stoss slope of sand dunes: limitations of current understanding. *Geomorphology* **17**: 47–54.
- Gillette DA, Adams J, Endo A, Smith D, Kihl R. 1980. Threshold velocities for input of soil particles into the air by desert soils. *Journal of Geophysical Research* **85**: 621–630.
- Greeley R, Iversen JD. 1985. *Wind as a Geological Process on Earth, Mars, Venus and Titan*. Cambridge University Press: New York.
- Hanjalic K, Launder BE. 1972. A Reynolds stress model of turbulence and its application to thin shear flows. *Journal of Fluid Mechanics* **52**: 609–638.
- Harlow FH, Nakayama PI. 1968. *Transport of Turbulence Energy Decay Rate*. Report. LA-3854, Los Alamos Science Laboratory.
- Howard AD. 1977. Effect of slope on the threshold of motion and its application to orientation of wind ripples. *Bulletin Geological Society of America* **88**: 853–856.
- Iversen JD, Rasmussen KR. 1994. The effect of surface on saltation threshold. *Sedimentology* **41**: 721–728.
- Jackson PS, Hunt JCR. 1975. Turbulent wind flow over a low hill. *Quarterly Journal of the Royal Meteorological Society* **101**: 929–955.
- Lancaster N, Nickling WG, McKenna Neuman C, Wyatt VE. 1996. Sediment flux and airflow on the stoss slope of a barchan dune. *Geomorphology* **17**: 55–62.
- Launder BE, Morse A, Rodi W, Spalding DB. 1972. The prediction of free shear flows: a comparison of six turbulence models. In *NASA Conference on Free Shear Flows*, Langley.
- McKenna Neuman C, Lancaster N, Nickling WG. 1997. Relations between dune morphology, air flow, and sediment flux on reversing dunes, Silver Peak, Nevada. *Sedimentology* **44**: 1103–1113.

- McKenna Neuman C, Lancaster N, Nickling WG. 2000. The effect of unsteady winds on sediment transport on the stoss slope of a transverse dune, Silver Peak, NV, USA. *Sedimentology* **47**: 211–226.
- Parsons DR, Walker IJ, Wiggs GFS. 2004a. Numerical modelling of flow structures over idealized transverse aeolian dunes of varying geometry. *Geomorphology* **59**: 149–164.
- Parsons DR, Walker IJ, Wiggs GFS, Ferguson RI, Garvey BG. 2004b. Numerical modelling of airflow over an idealised transverse dune. *Environmental Modelling and Software* **19**: 153–162.
- Phillips M. 1980. A force balance model for particle entrainment into a fluid stream. *Journal of Physics D: Applied Physics* **13**: 221–233.
- Phillips M. 1984. Threshold wind velocity for particle entrainment at sub-atmospheric pressures as on the planet Mars. *Atmospheric Environment* **18**: 831–835.
- Potter KN, Zobeck TM, Hagen LJ. 1990. A microrelief index to estimate soil erodibility by wind. *Transactions of the American Society of Agricultural Engineers* **33**: 151–155.
- Raupach MR, Lu H. 2004. Representation of land-surface processes in Aeolian transport models. *Environmental Modelling and Software* **19**: 93–112.
- Sarre RD. 1987. Aeolian sand transport. *Progress in Physical Geography* **11**: 157–182.
- Shao Y. 2000. *Physics and Modelling of Wind Erosion*. Kluwer Academic Publishers.
- Shao Y, Lu H. 2000. A simple expression for wind erosion threshold friction velocity. *Journal of Geophysical Research* **105**: 22437–22444.
- Walker IJ, Nickling WG. 2002. Dynamics of secondary airflow and sediment transport over and in the lee of transverse dunes. *Progress in Physical Geography* **26**: 47–75.
- Walker IJ, Nickling WG. 2003. Simulation and measurement of surface shear stress over isolated and closely spaced transverse dunes in a wind tunnel. *Earth Surface Processes and Landforms* **28**: 1111–1124.
- Wiggs GFS, Livingstone I, Warren A. 1996. The role of streamline curvature in sand dune dynamics: evidence from field and wind tunnel measurements. *Geomorphology* **17**: 29–46.
- Yakhot V, Smith LM. 1992. The renormalization group, the 3D-expansion and derivation of turbulence models. *Journal of Scientific Computing* **7**(1): 35–61.
- Zheng XJ, He L, Wu JJ. 2004. Vertical profiles of mass flux for windblown sand movement at steady state. *Journal of Geophysical Research* **109**: B01106.
- Zheng XJ, Xie L, Zou X. 2005. Exploration of probability distribution of velocities of saltating sand particles based on the stochastic particle-bed collisions. *Physics Letters A* **341**: 107–118.
- Zheng XJ, Xie L, Zou XY. 2006. Theoretical prediction of liftoff angular velocity distributions of sand particles in wind-blown sand flux. *Journal of Geophysical Research*, D11109. DOI: 10.1029/2005JD006164
- Zhou YH, Guo X, Zheng XJ. 2002. Experimental measurement of wind-sand flux and sand transport for naturally mixed sands. *Physical Review E* **66**: 021305–021305.9.